



Review

A Review: Recent Progress in the Design and Development of Nonlinear Radars

Ashish Mishra  and Changzhi Li  *

Department of Electrical and Computer Engineering, Texas Tech University, Lubbock, TX 79409, USA;
ashish.mishra@ttu.edu

* Correspondence: changzhi.li@ttu.edu

Abstract: This paper presents an extensive review of nonlinear response-based radar systems. Nonlinear radars are generally used for clutter suppression purposes. These radars detect the nonlinear response generated by diodes and transistors used as a tag for target localization. Utilizing the nonlinearity properties of these devices, these radars have been used for purposes including locating humans trapped in earthquakes and avalanches, identifying migratory patterns of animals, examining the flight pattern of bees, and detecting bugs in electronic devices. This paper covers the utilization of these radars in human vital signs monitoring, detecting targets in a clutter-rich environment, etc. State-of-the-art nonlinear radars' high-level architectures, design challenges, and limitations are discussed here. Recent works and results obtained by the authors are also summarized.

Keywords: harmonic; intermodulation; sub-harmonic; clutter rejection; nonlinear radar



Citation: Mishra, A.; Li, C. A Review: Recent Progress in the Design and Development of Nonlinear Radars. *Remote Sens.* **2021**, *13*, 4982.
<https://doi.org/10.3390/rs13244982>

Academic Editor: Gregory J. Mazzaro

Received: 27 October 2021

Accepted: 3 December 2021

Published: 8 December 2021

Publisher's Note: MDPI stays neutral with regard to jurisdictional claims in published maps and institutional affiliations.



Copyright: © 2021 by the authors. Licensee MDPI, Basel, Switzerland. This article is an open access article distributed under the terms and conditions of the Creative Commons Attribution (CC BY) license (<https://creativecommons.org/licenses/by/4.0/>).

1. Introduction

Conventional radars based on CW and FMCW modes cannot differentiate the target of interest from clutter based on the received signal. They require additional signal processing techniques such as characteristic motion, range/Doppler, or angular information for target discrimination and clutter suppression [1]. Nonlinear radar technology has been widely utilized for tracking smaller objects in the presence of large clutter, such as monitoring the dispersal of tagged insects. The tag contains an antenna and a nonlinear device such as a Schottky diode, which absorbs the radar's transmitted signal and uses it as an energy source, and re-emits nonlinear responses of the transmitted frequency. This type of nonlinear radar was commercialized by RECCO, which utilizes harmonic response for locating human targets for search and rescue operations. The design of a radar system depends on the frequency band selection, which in turn depends on the environment for maximizing the signal-to-noise ratio (SNR), minimizing interference from neighboring devices, and generating good spatial resolution. In addition to frequency selection, the radar operation is dependent on transmitter power, receiver sensitivity, radar antenna gains, and algorithms for detecting desired objects. Nonlinear radars are designed to detect hidden electronics, track very small things in the presence of large clutter, and the suppression of large undesired motions to detect small-amplitude motions.

This paper presents a detailed review of the existing nonlinear radars (harmonic, subharmonic, and intermodulation radars), the design requirements, and the challenges of developers and users. A generic system-level design of these radars is discussed, and the performance achieved by these nonlinear radars is compared. Special attention is given to those radars that deal with detecting passive electronic devices. The paper culminates by describing the recent advances based on the author's recent work in nonlinear radars in mapping targets in a clutter rich environment, target motion detection, device authentication, and monitoring vital signs, i.e., suppressing breathing/modifying the Doppler frequency return signal compared to a weak heartbeat signal on the hardware.

The paper is divided into six sections. A brief comparison between the nonlinear radar and conventional radar path loss model and sensitivity issues are discussed in Section 2; Section 3 gives an overview of the subharmonic radar system; Section 4 describes the harmonic radar systems and their current progress, and Section 5 discusses the intermodulation radar. A conclusion is drawn in Section 6.

2. Nonlinear Radars Path Loss Model and Sensitivity Issues

The traditional radar range equation to detect the power level received by the radar from a target at a distance R with a radar cross-section σ is:

$$P_r = \frac{P_t \times G_T \times G_R \times \sigma \times \lambda_t^2}{(4\pi)^3 \times R^4} \quad (1)$$

where P_t is the power level of the transmitted signal, G_T and G_R are the antenna gain of transmitter and receiver, respectively, and λ_t is the wavelength of the fundamental response. In conventional radars, the received signal is dependent on the radar cross-section (RCS) of the target, i.e., the larger the RCS, the larger the received signal strength. However, the received power as a function of RCS does not apply to nonlinear radar because the frequency change takes place at the target end, i.e., the fundamental frequency that is transmitted is converted to nf , f/n or $mf_1 \pm nf_2$. The power level of the nonlinear response is dependent on the conversion loss provided by the tag at the target. This generated nonlinear response is sent back to the radar's receiver. This implies that a small tag with optimum conversion loss may reflect more nonlinear response than a large tag with a high conversion loss. Hence, the path loss model of the nonlinear radar can be estimated using the Friis transmission equation as:

Radar to tag:

$$P_{rt1} = \frac{P_{t1} \times G_T \times G_{rt} \times c^2}{(4\pi \times R \times f_1)^2}; P_{rt2} = \frac{P_{t2} \times G_T \times G_{rt} \times c^2}{(4\pi \times R \times f_2)^2} \quad (2)$$

Conversion loss at the tag:

$$P_{tt} = \alpha \times f(P_{rt1}, P_{rt2}) \quad (3)$$

Tag to radar:

$$P_r = \frac{P_{tt} \times G_R \times G_{tt} \times c^2}{(4\pi \times R \times NR)^2} \quad (4)$$

where P_{rt1} , P_{rt2} are the power levels of the fundamentals received at the tag for frequencies f_1 and f_2 having transmitted power level at P_{t1} and P_{t2} , c is the speed of light, P_{tt} is the power level of the nonlinear response generated by the tag with a conversion loss of α , and G_{rt} and G_{tt} are the gain of the tags receiving and transmitting antennas. For a single tone transmission model, f_1 can be replaced as f and P_{rt2} can be ignored. In Equation (4), NR denotes the frequency of the nonlinear response, i.e., nf , f/n or $mf_1 \pm nf_2$. Here, n denotes the order of division for the fundamental frequency for the f/n response; for the harmonic response nf , n denotes the order of harmonics and $m + n$ is the order of intermodulation response.

One of the significant issues in radar design is to achieve the desired sensitivity for the intended application. To enhance the sensitivity of the radar, two methods are used from a system point of view: increasing the transmit power of the radar and increasing the received signal power. For the first method, the power level is generally amplified by connecting a power amplifier in the transmitter section. However, the utilization of a power amplifier results in the generation of nonlinear responses. The generation of these nonlinear responses would provide false alarms and result in tracking clutter objects in the vicinity. Therefore, to avoid false alarms, filters or diplexers are generally utilized to suppress these unwanted responses below the noise floor in the transmitter section to

prevent them from being radiated. In the second method, the RF amplifiers and LNAs are used to boost the signal level in the receiver. However, the gain provided by these amplifiers covers a wide range. Thus, an amplifier that is designed to operate in the 2nd harmonics frequency range may also provide some gain to the fundamental response, thus leading to the generation of the 2nd-order harmonics from the fundamental and result in detecting the clutter. Usually, in order to deploy amplifiers in the receiver section, diplexers and filters are necessary. This issue is more pronounced in the intermodulation bases of nonlinear radars, where the fundamental and intermodulation responses lie within the same band. Therefore, the diplexers are generally preferred here because the roll-off factor for the diplexers is more significant than that of the filters.

The sensitivity requirements for the sensor depend on the application and the maximum range that the radar needs to measure. For indoor applications, generally -70 dBm sensitivity can be used to detect 1 mm motion at a distance of 1 m in the 5.8 GHz ISM band for a transmit power of approximately 0 dBm. The radar's sensitivity can be further improved by boosting the down-converted signal with a baseband amplifier with high gain. It should be noted that the baseband amplifier can only help in reducing the impact of quantization noise but not the SNR of the signal captured by the radar receiver.

Table 1 provides a brief comparison among the three nonlinear radar types. The subharmonic radars require active tags, thus making them useful for applications that need short time tracking, which is limited by the battery life. Moreover, the subharmonic response has a lower frequency compared to the fundamental; this results in a larger tag size, which makes it challenging to track smaller targets such as insects. In contrast, the harmonic and intermodulation tags are passive and have smaller tag sizes, making them ideal for monitoring small targets.

Table 1. Comparison among the three types of nonlinear radars.

| Features | Subharmonic Radar | Harmonic Radar | Intermodulation Radar |
|-------------------------------|----------------------------------------------------------------------------------------|------------------------------------------------------------------------------------------------------------------------------------------------|----------------------------------------------------------------------------------------------------|
| Nonlinear response | $\frac{f}{2}, \frac{f}{4}$, etc. | $2f, 3f$, etc. | $2f_1 - f_2, 2f_2 - f_1$, etc. |
| Antenna | Dual-band | Dual-band | Single-band |
| Licensing issue | Yes | Yes | No |
| Pathloss * | At least 6 dB lower than fundamental | At least 6 dB more than fundamental | Same as fundamental tones |
| Tag type | Active | Passive/Active | Passive/ Active |
| Tag design | N/A | Matching circuit for dual-band operation | Matching circuit for single-band operation |
| Lifetime | Battery life | Wear and tear (Passive) | Wear and tear (Passive) |
| Components for tag | Frequency divider, battery, and antenna | Schottky diode, matching circuit, and antenna | Schottky diode, matching circuit, and antenna |
| Realization at high frequency | Easy | Fairly easy | Difficult |
| Applications | Tracking large targets for a smaller time duration, human vital signs monitoring, etc. | Tracking small and large targets for longer duration, migratory pattern of animals, vital signs monitoring, detecting hidden electronics, etc. | Tracking targets for longer duration, authentication of devices, vital signs, mapping target, etc. |

* antennas having equal gain.

3. Subharmonic Radar System

The subharmonic radar systems transmit as fundamental frequency waveform f in the environment. The tag for these radar systems captures this frequency and retransmits an additional f/n towards the radar receiver. The receiver of these radars is tuned to pick up these f/n frequency responses. Here, n denotes the order of division for the fundamental frequency. Figure 1 shows the typical block diagram of subharmonic radar systems. These radars typically require active tags for converting the fundamental into their subharmonic frequency responses; this, in turn, limits the lifecycle of the tag. In these radars, the path loss is reduced at the cost of a larger receiver size.

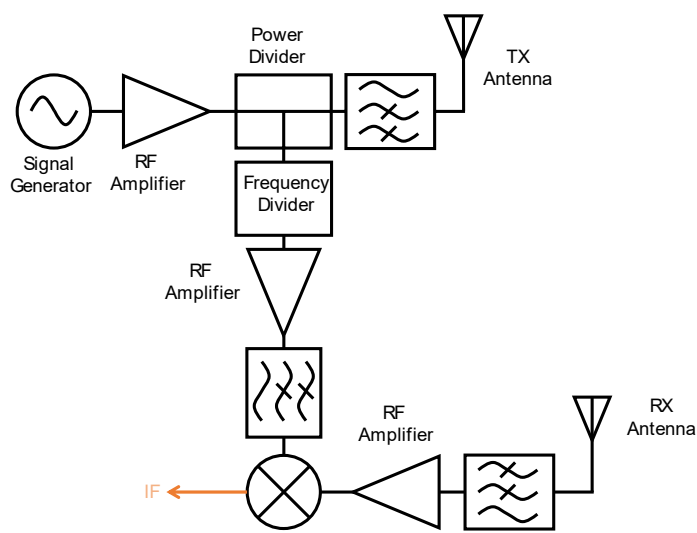


Figure 1. A block diagram of a subharmonic radar system.

A frequency tone transmitted by the antenna is denoted as:

$$T(t) = \cos[2\pi f t + \phi(t)] \quad (5)$$

where ϕ is the phase noise of the voltage-controlled oscillator (VCO) and t is the time. These transmitted tones are sent out and captured by the tag. The tag converts the transmitted tone as:

$$R(t) = \cos\left[\frac{2\pi f t}{n} - \frac{4\pi x_0}{\lambda} - \frac{4\pi x(t)}{\lambda} - \phi\left(t - \frac{2x_0}{c}\right)\right] \quad (6)$$

In Equation (6), λ represents the wavelength corresponding to f/n , $x(t)$ is the mechanical displacement of the tag, and x_0 is the nominal distance between the target and the radar. The transmitted signal passes through a frequency divider which divides the transmitted frequency by n before it is fed to the *LO* port of the mixer; hence the *LO* port signal can be written as:

$$L(t) = \cos\left[\frac{2\pi f t}{n} + \phi(t)\right] \quad (7)$$

The tag transmits it back to the radar. The desired subharmonic tone is amplified and down-converted at the mixer while attenuating the undesired frequency waveforms. The mixer down-converts the received frequency tone with a copy of the tone at *LO*, and the down-converted tone is represented as:

$$B = \cos\left[\frac{4\pi x_0}{\lambda} + \theta_0 + \frac{4\pi x(t)}{\lambda} + \Delta\phi(t)\right] \quad (8)$$

where θ_0 denotes the phase shift when the signal is backscattered by the tag and propagates along the receiver chain. $\Delta\phi(t)$ is the residual phase noise and can be ignored because the same signal generator is used for RF and *LO* signals, and a similar frequency multiplier is used in the *LO* and the tag.

In [2,3], a radar was discussed transmitting a 24 GHz ISM frequency waveform while the received subharmonic signal fell in the 2.4 GHz ISM band. The radar was operated in bandwidth BW , so the received subharmonic response was $BW/10$; hence, this radar type limits the range resolution of the radar at the cost of lower path loss and improved phase noise. Ref. [2] was used to measure a range up to 5 m. The accuracy for the radar was 22.3 cm and precision was 5.8 cm. Ref. [3] describes a subharmonic radar operating at 24 GHz/2.4 GHz for indoor localization purposes. The authors mentioned the accuracy was a few tens of cm. The radar transmitted approximately 4 W power, and the minimum sensitivity of the radar was -50 dBm.

4. Harmonic Radar System

Harmonic responses are generated when a fundamental frequency tone(s) is passed through nonlinear devices such as diodes, mixers, or transistors. There has been extensive research in this area of nonlinear radars for target localization in the presence of surrounding clutter. A harmonic radar-based localization system has been commercialized by a Swedish company, RECCO, which uses this harmonic response concept for search and rescue operations. The human targets wear tagged clothing, skiing equipment, and watches, which generate a harmonic response when energized by the signal transmitted from the RECCO detector systems. The harmonic response is generated at nf when a fundamental frequency f is passed through a nonlinear device. The order of the harmonic response is determined by n , where n is 2, 3, 4, etc. Most harmonic radars are based on n equals two responses as the 2nd order harmonic response has the highest power level among the harmonic responses. Figure 2 shows the block diagram of a harmonic radar system. Figure 3 shows model of a passive tag with antenna and some of the backscatterer types uses with harmonic radar.

A frequency tone transmitted by the antenna is denoted as:

$$T(t) = \cos[2\pi ft + \phi(t)] \quad (9)$$

where ϕ is the phase noise of the VCO and t is the time. The transmitted tone reaches the tag's antenna, which absorbs this transmitted tone and sends out a series of harmonic tones and the fundamental, i.e., $T(t)$, towards the radar receiver. The nonlinear response generated by the tag is denoted as:

$$R(t) = \cos\left[2\pi nft - \frac{4\pi x_0}{\lambda} - \frac{4\pi x(t)}{\lambda} - \phi\left(t - \frac{2x_0}{c}\right)\right] \quad (10)$$

In Equation (10), λ represents the wavelength corresponding to nf , $x(t)$ is the mechanical displacement of the tag, and x_0 is the nominal distance between the target and the radar. The transmitted frequency signal passes through a frequency multiplier which multiplies the transmitted frequency by n before it is fed to the *LO* port of the mixer; hence the *LO* port signal can be written as:

$$L(t) = \cos[2\pi nft + \phi(t)] \quad (11)$$

The radar receiver is tuned to the harmonic response, which is mostly 2nd order, and attenuates the other nonlinear responses and fundamental tone. The desired harmonic response is amplified and sent to the mixer for down-conversion purposes. After down-conversion, the baseband signal is obtained and forwarded to the ADCs for recording on a PC. The baseband response can be written as:

$$B = A \cos\left[\frac{4\pi x_0}{\lambda} + \theta_0 + \frac{4\pi x(t)}{\lambda} + \Delta\phi(t)\right] \quad (12)$$

The harmonic radars are the most widely used nonlinear radar due to their straightforward design and implementation. The wide separation of fundamental and harmonic response relaxes the filter and diplexer requirement compared to the intermodulation-based nonlinear radar. Ref. [4] discusses the relation between dipole orientation and length with the maximum detection range. The radar was designed to operate in 917/1834 MHz and used for tracking insects. Here, a study was performed discussing the effect of dipole length and bending on the dipole with the maximum detection range. Here the dipole was used as the tag's antenna. Ref. [5] presented the experimental and simulation-based validation of introducing an inductive loop across the diode terminals. Comparisons were performed for dipole lengths of free and fixed ends on the range, and a harmonic cross-section of the tag as a function of dipole length. In [6], a harmonic radar operating at 5.9–6 GHz/11.8–12 GHz is discussed. A modified Minkowski loop tag was used, which

provided improved harmonic conversion efficiency. The radar was able to detect insects at up to 58 m for 20 dBm output power.

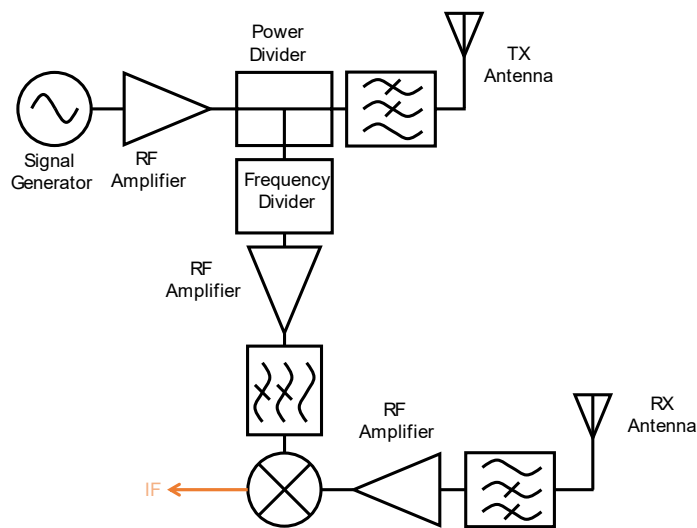


Figure 2. A block diagram of a harmonic radar system.

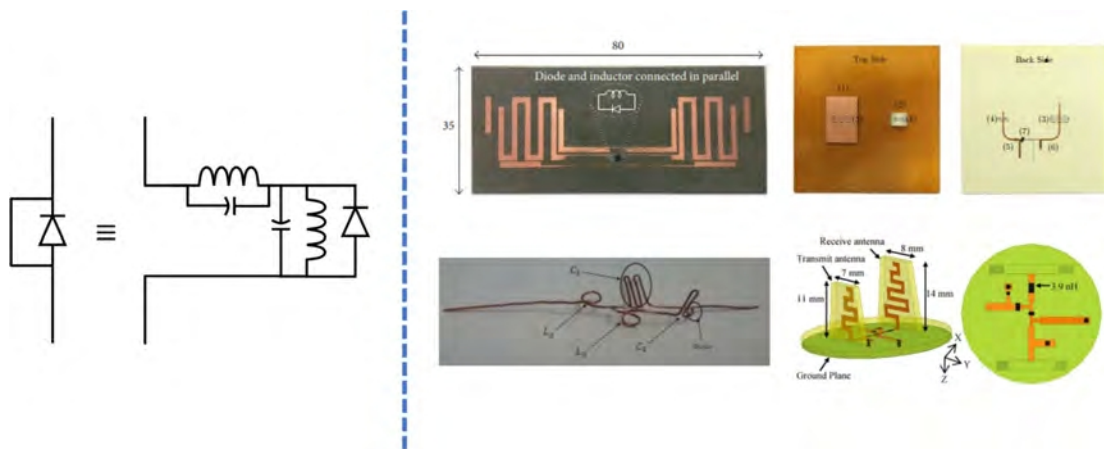


Figure 3. A model of a passive tag with a dipole antenna and a wire loop across the diode terminals and some common types of tags [Rasilainen, K. et al. (2015); Kubina, B. et al. (2018); Nourshamsi, N. et al. (2020); Nassar, I.T. et al. (2014)]. Reproduced with permission from Kubina, B., Mandel, C., Schüßler, M., Jakoby, R., Compact quasi-chipless harmonic radar sensor with a dielectric resonator antenna published by IEEE, 2018, Nourshamsi, N., Hilton, C., Vakalis, S., and Nanzer, J. A., Harmonic Micro-Doppler Detection Using Passive RF Tags and Pulsed Microwave Harmonic Radar published by IEEE, 2020 and Nassar, I. T., and Weller, T. M., A Compact Dual-Channel Transceiver for Long-Range Passive Embedded Monitoring published by IEEE, 2015.

In [7], a multitone harmonic radar is discussed, which utilizes harmonic response for detecting electronic components. Ref. [8] provides an overview of factors that should be taken into consideration when designing a harmonic radar. It discusses the impact of wavelength, radar transmission waveform, and choice of radar configuration. For example, it is noted that for tracking low flying insects, an azimuthally scanning harmonic radar is preferred over the point-and-track-based approach. Racal-Decca 90, a marine radar, was modified and utilized as a harmonic radar. Here the radar was transmitting 25 kW power with an antenna gain of 41.6 dB to track honeybees. Honeybees were tagged with a passive transponder containing a dipole antenna and a Schottky diode. Ref. [9] discusses the use of harmonic radar for tracking butterflies in an agricultural field. The radar can track insects at a maximum distance of 1210 m with a standard

error of approximately 455 m. In [10], the authors suggested some of the improvements that can be performed in the detection efficiency of targets using harmonic radars. The range resolution of harmonic radar using pulsed radar can be improved by utilizing shorter pulses. Similarly, the frequency modulated continuous wave radar (FMCW) can improve the results by transmitting a frequency with bandwidth $two\Delta f$, unlike the value of Δf for the same chirp duration. The most commonly used antenna for the harmonic transponder is dipole or monopole, which require strict orientation, i.e., they need to be stiff and straight either in a vertical or horizontal orientation to minimize the cross-polarization loss factor. These dipole or monopole antennas can be replaced with printed circuit antennas; the frequency doubler can be an externally biased energy source, such as a small piezo transducer or micro-cell, because the unbiased doubler has considerably larger conversion loss. Ref. [11] discusses the study of tagged bees in a range of within 700 m using the harmonic radar. Their flight patterns were recorded. In [12], the authors proposed harmonic radar with pseudorandom code (PRN code) positioning techniques; this is a spread spectrum technique for simultaneously achieving high sensitivity and accuracy. In PRN code, pulse compression is performed to accurately estimate the delay between the transmit and received signal. In comparison with other coding methods, such as Barker code and Gold code, the PRN code techniques can be generated with relatively ease and high accuracy. In [12], the radar operated at 9.4 GHz/18.8 GHz, with a 1.75 W power level; the radar was able to detect targets at a range of up to 60 m, and with 3 kW output power, 900 m detection was expected with an accuracy of 7.5 cm.

Refs. [13–15] discussed the use of harmonic radar for measuring the vital sign information of human targets. In [14], the radar was operated in 12/24 GHz frequency in continuous wave (CW) mode. The measurements were performed to validate the suppression of flicker noise and improvement of signal-to-noise ratio (SNR) compared to the conventional radar operating in the fundamental and harmonic frequency region. Ref. [15] utilized a CW-mode harmonic radar in the 2.45/4.9 GHz band. Multiple measurements were performed to validate the clutter motion rejection ability of the radar.

In [16], a marine radar transmitting 25 kW power was used as a transmitting module for the harmonic radar. The transmitting antenna had a gain of 28.5 dBi, whereas the receiving antenna had a gain of 27.4 dBi and was connected to LNAs and power amplifiers. The radar was operated in pulsed mode and sent at a frequency of 9.41 GHz. The receiver was tuned to run at 18.82 GHz. Tags with different antenna orientation around the Schottky diode were analyzed to validate the performance of different tag types such as loop and cross across the diode. The radar was able to detect targets at a range of up to 125 m. In [17], upgrades were undertaken to work performed in [16], such as introducing a waveguide WR90 filter in the transmitter section to reduce the harmonics at 18.82 GHz from being transmitted, and replacing the horizontally polarized antenna with a vertically polarized antenna. The antenna gain for transmitter and receiver sections was 26.6 and 27.3 dBi, respectively. The mounting procedure and shape of the tag were further optimized. The radar was then able to detect targets at a range of up to 150 m. Ref. [18] discusses the harmonic radar working at 9.4 GHz/18.8 GHz with 1 kW transmitting power for detecting targets at a range of up to 500 m. Compared to the previous loop or cross-shaped tag, the tag was modified into a "J" shape having arms with unequal length.

In the work in [19], a two-tone harmonic radar design is discussed. The system had a single antenna serving the role of both transmission and receiving antennas. A low-pass filter was used in the transmitter section to attenuate any harmonics generated by the amplifiers. A high-pass filter was used in the receiver section to attenuate the fundamental response. However, in this work, the received signal was not down-converted; instead, the received signal was measured on a spectrum analyzer. In [20], the fundamental frequency response f_0 was swept across a wide frequency band, and the amplitude and phase of the harmonic response for each $2f_0$ was recorded to determine the nonlinear response of the environment. An inverse fast Fourier transform (FFT) was performed on the nonlinear frequency response to determine the target range. In this work, ranging and detection was

performed on three nonlinear targets. Here, the radar was operated in a 700–900 MHz frequency region with a transmit power level of 2 W, and the ranging was performed to targets located at 12 ft. In [21], linearization techniques for a harmonic radar are discussed. Two linearizing methods are discussed: (a) filtering and (b) feed-forward cancellation. In the filtering method, system-generated nonlinear responses are removed by either attenuating or reflecting at the output of the nonlinearity. In the case of the feed-forward cancellation circuit, the undesired signal is combined with the signal path with a phase offset to remove it. The filtering technique can be implemented in both the transmitter and receiver sections, whereas the feed-forward process is generally implemented in the transmitter section. Its implementation is not usually practical in the receiver for a moving target and clutter. Synthetic aperture radar (SAR) images of linear and nonlinear targets were measured from the harmonic and conventional radars in [22]. The nonlinear radar was able to suppress the clutter, i.e., linear target, and detect a nonlinear target. In contrast, the conventional radar was able to pick the signature of both types of targets. Ref. [23] discusses the filters that are used in radar. The paper discusses the change in the measured and theoretical results when low-pass filters are cascaded. Measurements were performed when the filters were connected without and with a cable. The oscillation in the stopband was more when the filters were cascaded with a cable between them. However, when the cascading was performed for the diplexers with and without a cable, the theoretical and measured values matched. This is due to the reflective behavior of the filters, which changes the S_{21} characteristic when cascaded. The receiver for a harmonic response is designed to reflect the fundamentals while allowing the harmonics to pass through. However, some of the fundamentals still leak from the RF devices. The nonlinearity presents in the RF devices, such as LNAs and amplifiers, can generate a harmonic response from the fundamental frequency and result in false alarms [24]. Ref. [24] utilizes states in which diplexers can be used to minimize the reflection of the unwanted frequency and thus help in improving the false alarm condition. In work [25], harmonic radar was operated in the pulsed on-off mode, and the relation between duty cycle and power level of nonlinear response was determined for fixed incident power level. From measurements and simulations, it was found that the lowest duty cycle produces the maximum average target harmonic response. Ref. [26] discusses the implementation of a harmonic radar transmitting a fundamental frequency from 800 to 1000 MHz and receiving harmonics at 1600–2000 MHz for imaging moving targets and obtaining SAR images of the targets in the presence of clutter. Ref. [27] discusses the integration of harmonic radar with a Transverse Electromagnetic (TEM) cell. Here, the fundamental tone was radiated into the TEM cell containing the nonlinear target. In [28], passive filtering is discussed. The characteristics that should be possessed by a filter to enable utilization in a harmonic radar are discussed, e.g., the passband for filters in the receiver and transmitter should not overlap; for the filter in the transmitter, the attenuation at harmonic frequency should be at least 50 dB and close to 0 dB at the fundamental. Similarly, filters in the receiver should provide more than 70 dB attenuation to fundamental, while it should be close to 0 dB for harmonics.

Harmonic radars were implemented in studying the flight behavior pattern of infected honeybees [29]. Refs. [30–32] discuss the use of harmonic radar to track amphibians' behavior in a clutter-rich environment. The radar in [30,31] was operated in a 5.8 GHz ISM band for transmission and a 12 GHz satellite TV band for the reception for the nonlinear response.

In [33], a harmonic radar working at 9.4/18.8 GHz could detect targets up to a range of 500 m. In the transmitter section, on-off keying (OOK) modulation and binary phase-shift keying (BPSK) were performed. Various tag topologies were tested to obtain the optimum transponder. High-gain TX and RX antennas with gains of 26.6 and 27.3 dBi, respectively, were used in this radar. To obtain high range resolution and high sensitivity, short pulses with high power were used. To receive short high-power pulses, a pulse compression technique was used. The measurements were performed in a harsh outdoor environment, and the radar was able to track targets at a range of up to 500 m. Ref. [34] utilizes harmonic

radar for tracking slow-moving targets very close to the ground. The harmonic radar was operated in the 914/1828 MHz frequency band. The antenna in the transponder was designed to match the port impedance of the Schottky diode, which was used as a nonlinear device. Bow-tie and partial bow-tie antennas were used, and the maximum detection ranges of the tags were compared.

Ref. [35] discusses the non-linearities present on the radar sensor and the parasitic signal leakage from the transmitter to the receiver, which causes issues with tag detection. The passive tags have extremely low returns, so a weak parasitic harmonic response can negatively impact the system's performance. This work showed that in a pulsed harmonic system, the parasitic harmonic response can be compensated and eliminated in the delay domain. With a numerical evaluation, it was proven that it can result in improved tag detection. Ref. [36] discusses the various topologies of harmonic transponders that were designed. Based on the applications, there was some trade-off to achieve the desired characteristics using these harmonic transponders. Ref. [37] discusses the use of harmonic radar for tracking targets that can be installed on small UAVs. The system was designed to transmit the frequency in C-band and receive the frequency in X-band. In [38], a quasi-chipless temperature-dependent harmonic radar sensor is presented, which utilizes the response to determine the environment's temperature at up to 3.75 m. Ref. [39] provides theoretical and measurement validation of utilizing a two-tone signal and a dedicated receiver to overcome phase ambiguities caused by the short signal wavelength, and provided accurate localization in a multipath environment with clutter. The specific harmonic radar cross-section effect (SHRCS) concept depends on the power density of the backscatter from tags. Ref. [40] discusses the utilization of CW radar in frequency-hopping spread spectrum (FHSS) mode. The fundamental frequency was hopped between 30 points, and a similar 30 harmonic frequency was recorded from the tag to estimate the range. Ref. [41] discusses the use of harmonic radar in pulsed mode to estimate the distance of the target. The radar was operated in a 2.51/5.02 GHz band with a 16 dBm power level of the fundamental frequency. The matching circuit for the tag (capacitors and inductors) was realized using the wire bends. Measurements were performed for the maximum detection range as a function of the duty cycle.

Different electronic components can be distinguished from one another based on the nonlinear return signal. The nonlinear return signal strength is different for different nonlinear components; hence, based on the power level of the return harmonic signal mean, variance skewness, and kurtosis, various electronic devices were distinguished [42]. In [43], a series of harmonic responses from different devices were measured with respect to the change in the input power level. Fourier transform was performed on the returned harmonic responses to distinguish between different nonlinear devices.

Refs. [44,45] shows the implementation of a harmonic radar in the marine environment. The radar was implemented in stepped frequency continuous wave mode with an output power of ≈ 76 dBm in the S-/C-band. The radar was able to locate a passive target at a range of up to 750 m with a peak transmit power of 25 kW, and at about 5800 m for active tags.

Ref. [46] discusses the use of RECCO's harmonic radar for obtaining SAR images from Unmanned Aerial Systems (UASs). In that work, three different steps in obtaining the SAR image were performed. In the first, the ego disturbance was calculated where the UAS was positioned at an altitude over an isolated area where external disturbances were not present. In the second step, altitude profiling was performed; here, the altitude was determined at which the radar could detect the signal with high reliability. In the third and final step, the fixed altitude response mapping was performed where the UAS was flown around an area at a constant altitude of 8 m, and a reflector placed at a height 40 cm above the ground was mapped. Harmonic radars are mainly used to track small targets that are surrounded by large clutter. These radars are used to determine the flight patterns of pests, honeybees, and other small objects. Here, the size of the transponder plays a crucial role in accurately mapping their behavior. Large and bulky transponders affect their

behavior, so it is challenging to design small and light transponders which will not affect their movement pattern. Ref. [47] discusses the design of lighter transponder tags that can generate desired harmonic frequencies with optimum power levels for ranging purposes. In [48], a dual-channel harmonic transceiver operating at 2.4/4.8 GHz is discussed. Here the dual-channel design provides an omnidirectional interrogation capability. The harmonic repeater was enclosed in a sandy environment to validate its impact on the conversion gain and operating frequency of the radar. In [49], a graphene-based harmonic radar transponder, for implanting in the human body, is discussed.

Ref. [50] addresses the issue of the weak return signal from the harmonic transponder, which limits the range of harmonic radar. The most common approach to increase range is to increase the transmit power of the radar. However, the inverse sixth power dependence on the range in harmonic radar makes it an expensive approach. Here auxiliary transmission nodes are used, which results in a higher power at the receiver, thus increasing the radar's maximum range.

The harmonic radar discussed in the above works was based on detecting the 2nd order harmonic response from the tag. In [51], the authors designed a new harmonic radar to exploit the 3rd order harmonic response. Figure 4 shows the block diagram and system of the harmonic radar operating in the 24/72 GHz band. Figure 5 shows the passive tag that was used as a backscatterer for the radar. The 2nd order-based harmonic radar requires filters and diplexers for attenuating the 2nd harmonic in the transmitter and the fundamental in the receiver to avoid false alarms. However, because the fundamentals and the harmonics are far from one another, the devices working at the fundamental frequency band attenuate the 3rd order harmonics because the package matching does not support $3f$. Similarly, the receiver components do not support the f frequency region.

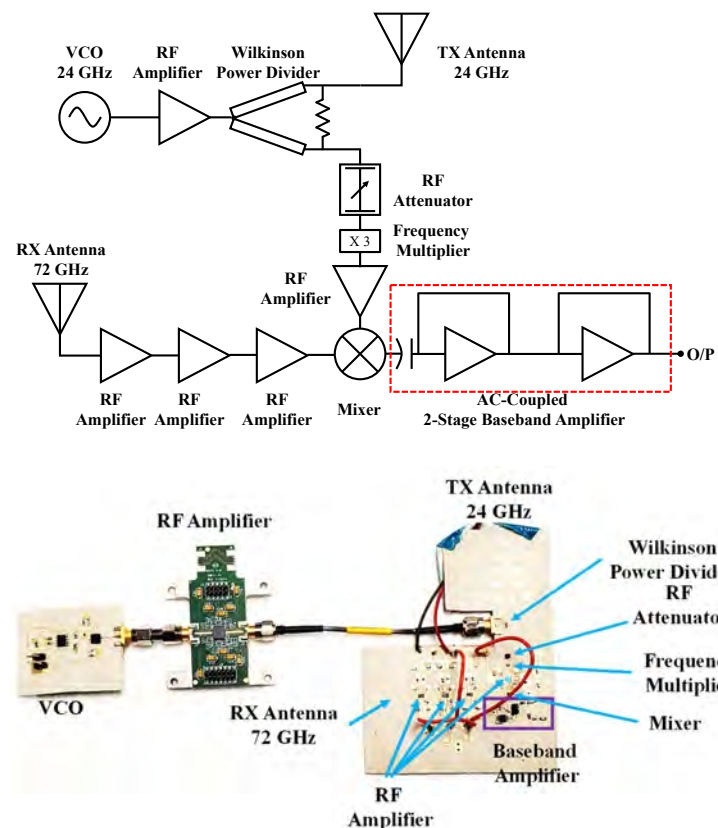


Figure 4. A block diagram and radar system of a 24/72 GHz harmonic radar system [51]. Reproduced with permission from Mishra, A., and Li, C., A third-order harmonic radar design for mm-wave frequencies published by SPIE, 2021.

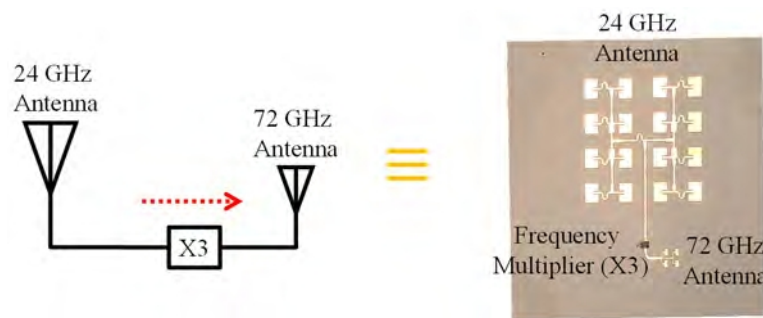


Figure 5. 24/72 GHz passive transponder [51]. Reproduced with permission from Mishra, A., and Li, C., A third-order harmonic radar design for mm-wave frequencies published by SPIE, 2021.

The experimental validation of the 3rd order harmonic radar was performed with two experiments, as shown in Figure 6. In the first experiment, tag and clutter, i.e., metal plates, were sequentially moving with equal motion amplitude and frequency. In the second experiment, the tag and clutter were moving simultaneously with unequal amplitude and frequency. The motion of the clutter was larger than the motion of the tag. The phantom shown in Figure 6 is a mechanical device used to mimic human breathing, and the actuator is a mechanical device used to produce sinusoidal motion, where the frequency and amplitude can be programmed. Figure 7a shows the result of the first experiment, and Figure 7b shows the result of the second experiment. Both of these experiments shows that the radar successfully suppressed the motion of clutter.

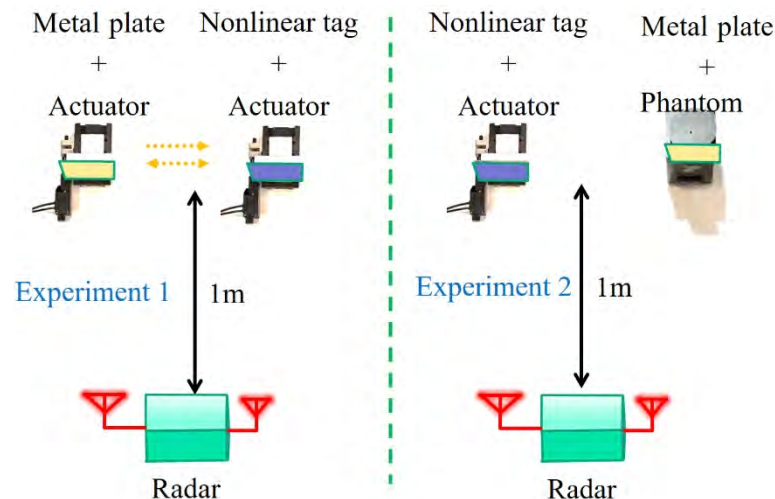


Figure 6. Experiments performed for clutter rejection validation [51]. Reproduced with permission from Mishra, A., and Li, C., A third-order harmonic radar design for mm-wave frequencies published by SPIE, 2021.

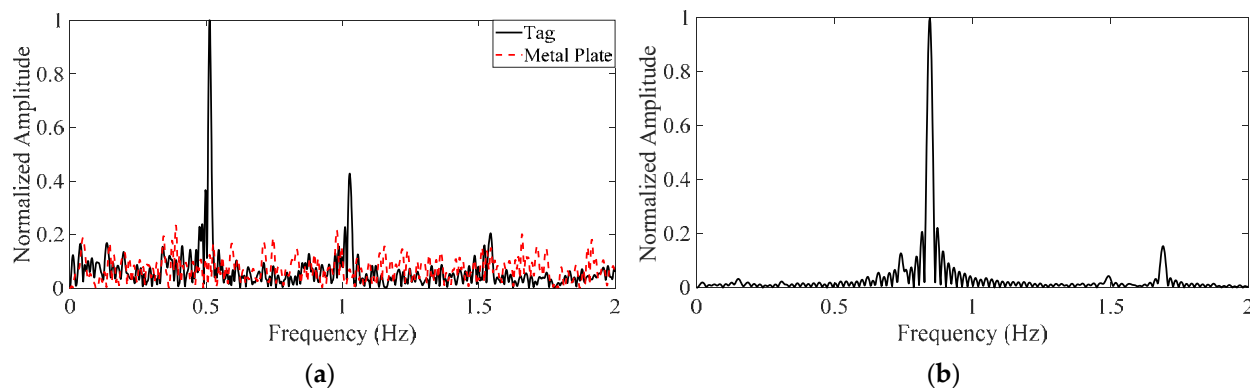


Figure 7. Measurement results: (a) FFT from data for Experiment 1; (b) FFT from data for Experiment 2 [51]. Reproduced with permission from Mishra, A., and Li, C., A third-order harmonic radar design for mm-wave frequencies published by SPIE, 2021.

5. Intermodulation Radar System

Harmonic and subharmonic radars have been studied extensively. They are relatively simple to design and implement. However, they suffer from issues such as licensing because the fundamental and harmonic/subharmonic responses lie in different frequency bands. Thus, the nonlinear tags require a matching circuit for optimum operation, and the harmonic tags therefore need matching for two bands, i.e., fundamental and harmonic. As a result, the matching circuit for harmonic radars is more complex compared to intermodulation-based tags where fundamental and desired nonlinear responses lie in the same band; thus, the matching circuit needs to be designed for narrowband operation.

When two or more frequency tones are passed through a nonlinear device, the device produces additional frequency tones in addition to fundamentals and harmonics. These additional tones are called intermodulation. The discussion here is limited to odd-order intermodulation products. These intermodulation products are produced at $mf_1 \pm nf_2$, where f_1 and f_2 are the two fundamental tones illuminating the nonlinear device. The order of the intermodulation is $m + n$. Figure 8 shows the block diagram of an intermodulation radar. Here, three signal generators are generally utilized: two signal generators to generate fundamental frequency tones f_1 and f_2 for transmitting into the environment, and a third signal generator at $mf_1 \pm nf_2$ for down-converting the received tones to extract Doppler or range information of the nonlinear target. Generally, the third signal generator is tuned to $2f_1 - f_2$ or $2f_2 - f_1$ as these frequency tones have the highest power levels among the nonlinear response within the same band.

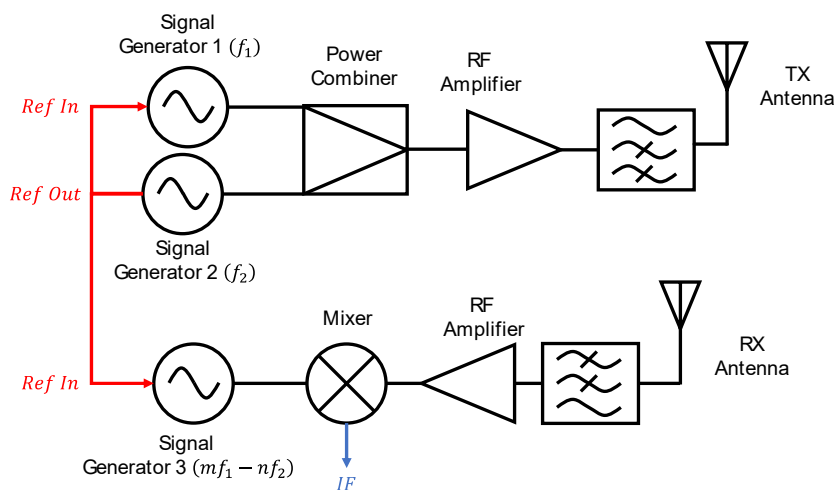


Figure 8. A block diagram of an odd order intermodulation radar system with $f_1 < f_2$.

The antenna transmits two or more frequency tones, denoted as:

$$T(t) = \sum_{i=1}^n \cos[2\pi f_i t + \varphi_i(t)] \quad (13)$$

where φ_i is the phase noise of the n signal generators, and t is the time. The transmitted tone reaches the tag's antenna, which absorbs this transmitted tone and sends out a series of intermodulation tones along with the fundamentals. The nonlinear response generated by the tag is denoted as:

$$R(t) = \cos \left[2\pi n f_{IM} t - \frac{4\pi x_0}{\lambda} - \frac{4\pi x(t)}{\lambda} - \varphi \left(t - \frac{2x_0}{c} \right) \right] \quad (14)$$

In Equation (14), λ represents the wavelength corresponding to f_{IM} intermodulation frequency, $x(t)$ is the mechanical displacement of the tag, and x_0 is the nominal distance between the target and radar. The transmitted frequency signal passes through a frequency multiplier which multiplies the transmitted frequency by n before it is fed to the *LO* port of the mixer; hence the *LO* port signal can be written as:

$$L(t) = \sum_{i=1}^n \cos[2\pi f_{IM} t + \varphi(t)] \quad (15)$$

The radar receiver is tuned to intermodulation response, which is mostly 3rd order, and attenuates the other nonlinear responses and fundamental tone. The desired intermodulation response is amplified and sent to the mixer for down-conversion purposes. After down-conversion, the baseband signal is obtained, and sent to the ADCs for recording on a PC. The baseband response can be written as:

$$B = \cos \left[\frac{4\pi x_0}{\lambda} + \theta_0 + \frac{4\pi x(t)}{\lambda} + \Delta\phi(t) \right] \quad (16)$$

Here, $\Delta\phi(t)$ is the residual phase noise and can be ignored for short distance approximation due to the range correlation effect [52]. Figure 9 shows the model of a passive diode-based tag and some of the tags utilized for this radar for ranging and motion detection in the presence of clutter.

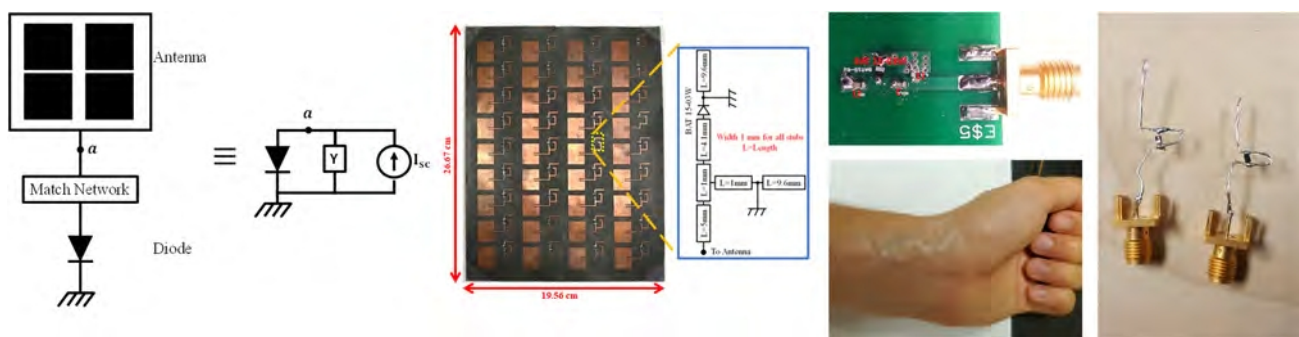


Figure 9. A model of a passive tag with an antenna and matching circuit across the diode terminals and some common types of tags [Mishra, A. et al. (2018); Mishra, A. et al. (2019)]. Reproduced with permission from Mishra, A., and Li, C., 5.8-GHz ISM band intermodulation radar for high-sensitivity motion-sensing applications published by IEEE, 2018.

Intermodulation-based radar has gained interest for its utilization in clutter rejection purposes. In [53], a contactless method of determining the radiation pattern of a transponder is discussed. In [54], an antenna working at a 77 GHz automotive band was designed to be used with an intermodulation radar. A simulation was performed to validate the target discrimination with an intermodulation radar. An RFID-based system based on

intermodulation response is discussed in [55]. Two tones were illuminated on the active tag, and backscatter from the tag was recorded. The RFID reader transmits frequencies at 2.4 and 2.46 GHz, and utilizes a 2.34 GHz return signal for validation.

In [56], for the first time, the intermodulation response was utilized for remote sensing of motion of clutter and a target. In this work, the intermodulation radar was designed and operated in a 5.8 GHz ISM band, and experimental validations were performed to determine the clutter rejection ability of the radar. A four-by-four antenna array was mounted on the phantom, and a long SMA cable was connected to it. The antenna array and phantom were made to move back and forth in front of the radar under three conditions when the SMA port was: open, connected to a $50\ \Omega$ load, and connected to the nonlinear device. The motion under the three conditions was recorded. Figure 10a shows the antenna's connection with the phantom, and the measurement result is plotted in Figure 10b. It can be seen from the measurement result that the motion frequency of the phantom could be recorded only then the antenna was connected with the nonlinear device, whereas in the case of open and load conditions, the measurement frequency could not be recorded.

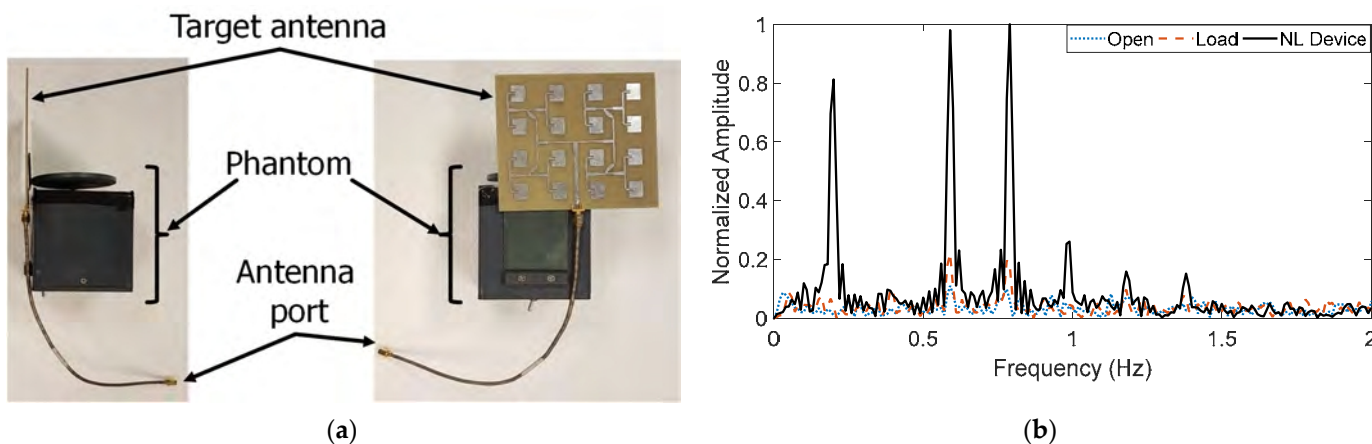


Figure 10. Mechanical motion discrimination: (a) Alignment of antenna with phantom; (b) FFT plot showing the Doppler frequency of the phantom's motion [56]. Reproduced with permission from Mishra, A., and Li, C., 5.8-GHz ISM band intermodulation radar for high-sensitivity motion-sensing applications published by IEEE, 2018.

The intermodulation responses were utilized in authenticating two similar devices having identical components and matching circuits. In work [57], the intermodulation return signal from the nonlinear device was recorded. Figure 11 shows the measurement setup for transmitting the fundamental response to the nonlinear targets and recording their fundamental and intermodulation return. Two signal generators were used to transmit the two frequency tones towards the power combiner, and the output of the power combiner was sent towards the circulator. The circulator was connected to send signals from Port 1 to Port 2 and Port 2 to Port 3. Thus, the nonlinear devices were connected sequentially to Port 2 and the return signal from these devices was recorded on a spectrum analyzer connected to Port 3. The fundamental return signals, when used for authenticating these two devices, have a minimal difference in power level. Thus, they were discarded; however, when the 3rd order nonlinear responses were utilized for differentiating these two devices, the power level trend showed a similar trend for most of the frequencies. At a particular frequency band, the difference in power level was significant. In this work, a power level difference of more than 10 dB was considered to be significant. Figure 11b shows the nonlinear return signal from the two devices from 4 to 10 GHz, with $\Delta(f_2 - f_1)$ as 10 MHz and a step size of 100 MHz. The power level was set as 5 dBm at 5 GHz for both tones.

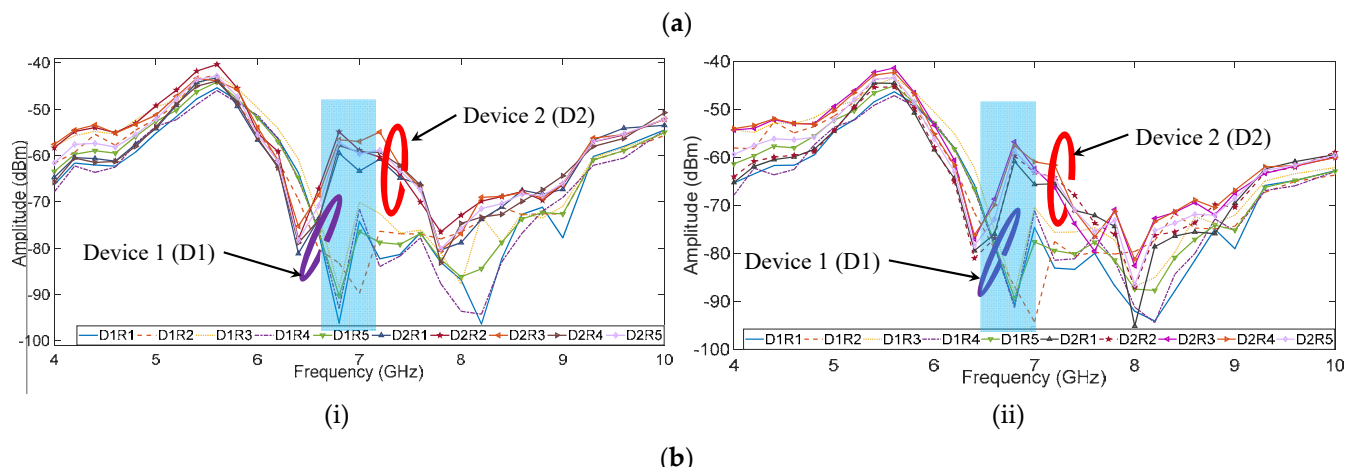
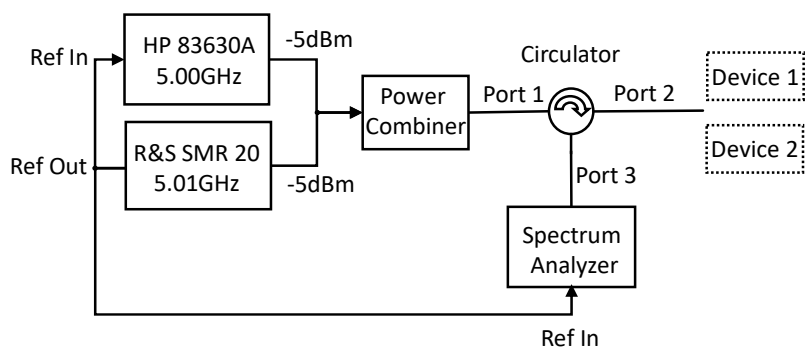


Figure 11. (a) A block diagram of an intermodulation-based authentication system [57]; (b) nonlinear return from nonlinear devices: (i) $2f_1 - f_2$, (ii) $2f_2 - f_1$. Reproduced with permission from Mishra, A., Song, C., Xu, W., and Li, C., Investigation of unique broadband nonlinear RF response of electronic devices published by IEEE, 2018.

In [56], the intermodulation-based radar was first designed, the motion frequency was recorded, and clutter rejection was first performed. However, in [56], due to the absence of a series of LNA and RF amplifiers, the radar's sensitivity was very low. This had an impact on the maximum distance and minimum motion amplitude the radar could measure, without linearizing the transmitter and section, and utilizing amplifiers and LNAs to boost the transmitted and received signal. As a result, the intermodulation radar was modified, and a series of amplifiers and LNAs were connected while maintaining or even improving the linearity of the radar system. The sensitivity was improved from -65 to -120 dBm. Figure 12 shows the system diagram of the 5.8 GHz ISM band intermodulation radar. Because the intermodulation radar required attenuating the unwanted tones within the same band, off-the-shelf filters could not be utilized since the roll-off feature needs to be very sharp. Thus, either custom filters have to be used, or diplexers are required. Filters need to be reflectionless because connecting two or more reflection-based filters does not provide the desired attenuation as theoretically calculated based on $S21$, and the reflection of the tones tends to alter the behavior of the filter. Hence, diplexers are preferred as the unwanted frequency is directed to a different path where a $50\ \Omega$ load is connected which absorbs it instead of reflecting it to the previous stage. Moreover, the diplexers provide a very steep roll-off. Hence, in [58,59], diplexers were utilized to attenuate any unwanted tones absorbed by the antenna or generated by the nonlinear components to provide the desired linearity and avoid false alarms. The radar was used to measure the vital signs of a human target. The goal of the experiment was to measure a stronger heartbeat pattern compared to respiration. In the case of the conventional radars, the breathing pattern is stronger compared to the heartbeat pattern because displacement of the lungs during the respiration process is much larger than the displacement of the heart during a heartbeat. Hence the harmonics of respiration peaks in the frequency spectrum overlap with the weaker heartbeat peaks and lead to loss of information. Thus, by making the respiration

weaker than the heartbeat, the information is not lost. The validity of the heartbeat signal was compared with reference data. Figure 13a shows the placement of the tag on the human target. Here, the tag was aligned to the heart location to record a stronger heartbeat pattern. Figure 13b shows a short-time Fourier (STFT) plot obtained from the radar data. It can be seen that the radar successfully recorded a stronger heartbeat pattern compared to respiration.

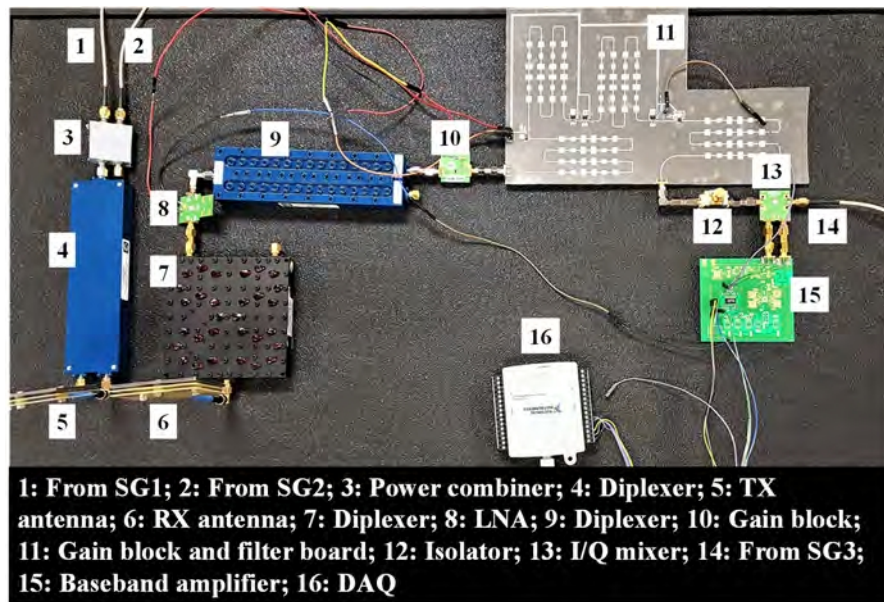


Figure 12. A modified intermodulation radar for measuring the Doppler frequency [58]. Reproduced with permission from Mishra, A., and Li, C., A Low Power 5.8-GHz ISM-Band Intermodulation Radar System for Target Motion Discrimination published by IEEE, 2019.

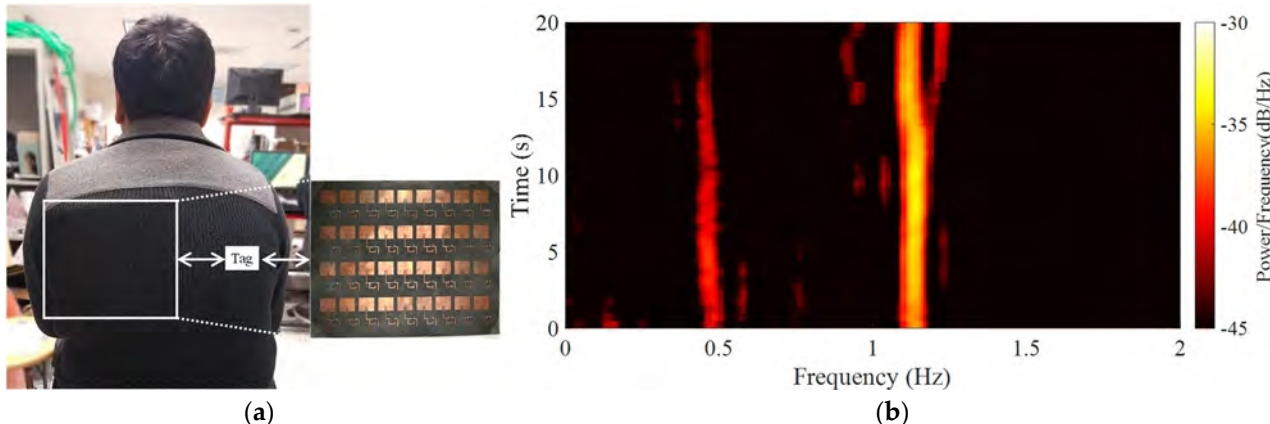


Figure 13. Utilizing the radar for measuring the vital signs of human target: (a) Tag placement on human target; (b) STFT plot showing vital signs of human target [58]. Reproduced with permission from Mishra, A., and Li, C., A Low Power 5.8-GHz ISM-Band Intermodulation Radar System for Target Motion Discrimination published by IEEE, 2019.

In [58,59], a thirty-six-element tag was used to record the strongest heartbeat pattern. However, this thirty-six-element tag is not practical to be utilized in all scenarios. Thus, a smaller tag was designed by placing a dipole antenna across the diode's terminals and a wire loop connecting both the diode's ends for biasing purposes [60,61]. The tag was placed on the wrist aligned to the radial artery. Figure 14a shows the placement of the tag on the wrist for measuring the heartbeat. The wrist was placed in front of the radar in the near-field region to measure the heartbeat pattern. Figure 14b shows the spectrogram obtained when the tag was placed on the wrist and kept in the near-field region. The plot

shows a strong heartbeat pattern. In [62], vital signs of the human target under different postures were recorded, such as sleeping, sitting with the wrist touching the torso, and sitting with the wrist not touching the torso. The radar was able to detect vital signs, especially heartbeat patterns, in all these scenarios. Error analysis was also performed on the heartbeat data recorded by the radar compared to the reference. It can be seen that the error was <10% under all the measurement scenarios.

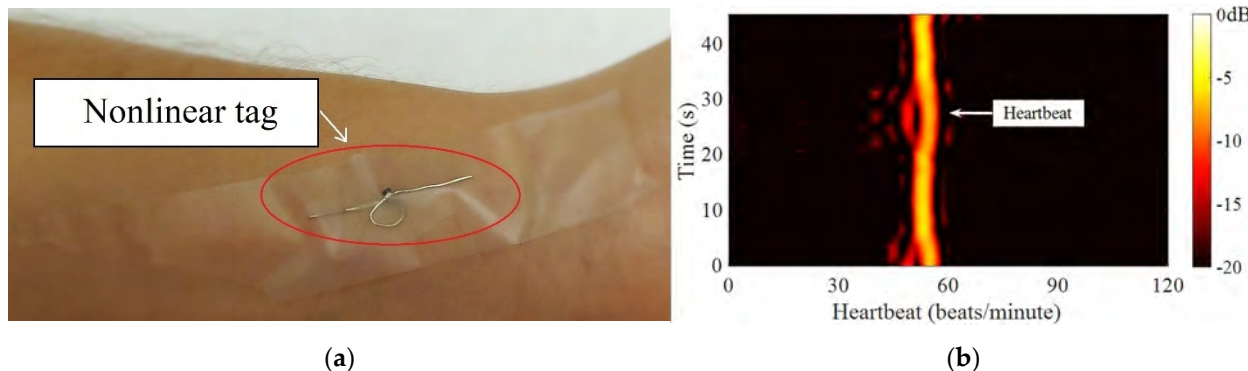


Figure 14. (a) A single passive nonlinear tag on the human wrist to measure the pulse/heartbeat pattern; (b) STFT plot of the data obtained when the tag on the wrist was placed in the near-field region [60]. Reproduced with permission from McDonnell, W., Mishra, A., and Li, C., Comprehensive Vital Sign Detection using a Wrist Wearable Nonlinear Target and a 5.8-GHz ISM Band Intermodulation Radar published by IEEE, 2020.

In the above works [53–60] on intermodulation-based nonlinear radars, only motion frequency could be obtained, and the radars could not be utilized for ranging purposes. In [61], the intermodulation radar was operated in frequency-shift-keying (FSK) mode. In this mode, f_1 of the tone was kept constant while f_2 of the tone was switched between two frequencies f_{2l} and f_{2h} ; thus, corresponding to the switching of f_2 , the lower 3rd order tone was generated at two frequencies, i.e., $2f_1 - f_{2l}(f_{IMLL})$ and $2f_1 - f_{2h}(f_{IMLH})$. A tag was placed on the target, so the tag backscattered the intermodulation response added with Doppler based on the incident fundamental tones. The radar sensor down-converts the received intermodulation response with a copy of the 3rd order tone at the I/Q mixer.

An FFT is performed on this down-converted signal, and the Doppler frequency peak of the target is identified for f_{IMLL} and f_{IMLH} return signals. The phase information is calculated from the FFT spectrum and the range of the target from the radar is determined using:

$$d = \frac{c\Delta\varphi}{4\pi\Delta f} \quad (17)$$

where c is the velocity of electromagnetic wave, $\Delta\varphi$ is the phase difference of the returned signal, and Δf is the $f_{IMLH} - f_{IMLL}$. Figure 15a shows the experiment setup where the range of the human target was determined based on the FSK modulation scheme. Unlike in previous intermodulation radars, where at least three signal generators with shared reference to maintaining coherence were utilized for operation, in [61], two signal generators were used. An external reference for maintaining the coherence was discarded; instead, a diode maintained the coherence between the fundamental and nonlinear response. Figure 15b shows the range measurement of a target for a 70 s duration.

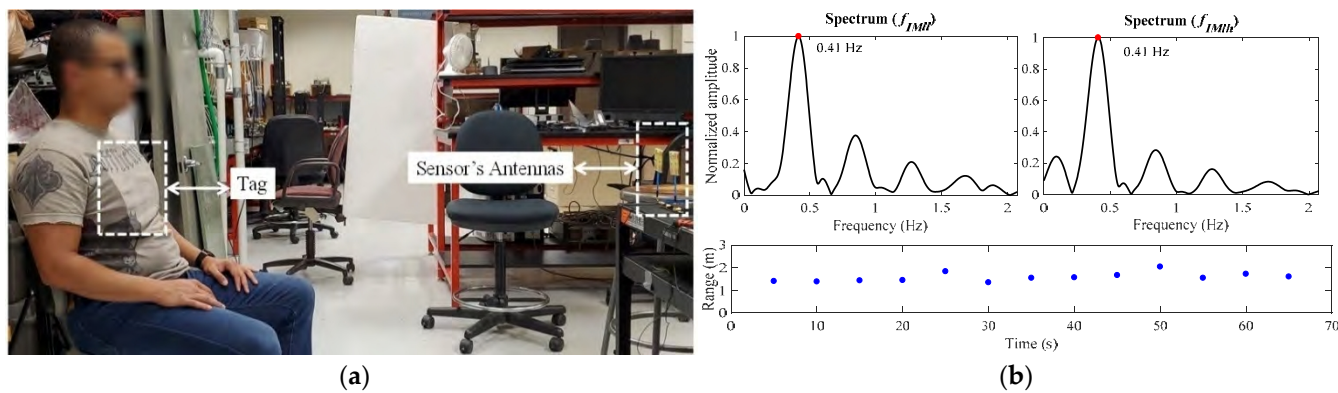


Figure 15. (a) Measurement scenario of intermodulation radar in FSK mode; (b) Range determination based on FSK mode [61].

In [62], the intermodulation radar was operated in frequency-modulated continuous-wave (FMCW) mode. Similar to FSK mode, one of the fundamental tones was swept with a bandwidth, which resulted in the generation of a 3rd order response to be generated with the same bandwidth in the opposite direction. Figure 16 shows the modulation scheme of the intermodulation response when one of the fundamental tones is swept. The radar was used for mapping targets in a clutter-rich environment, as shown in Figure 17a. The measurement obtained by this radar was compared with the state-of-the-art conventional FMCW radar, and the mapping result is plotted in Figure 17b. As shown in the figure, it can be seen that a conventional radar cannot discriminate between clutter and target. It records the location of all the objects present in its vicinity, whereas an intermodulation radar was successfully able to suppress the clutter response and record the location of the target.

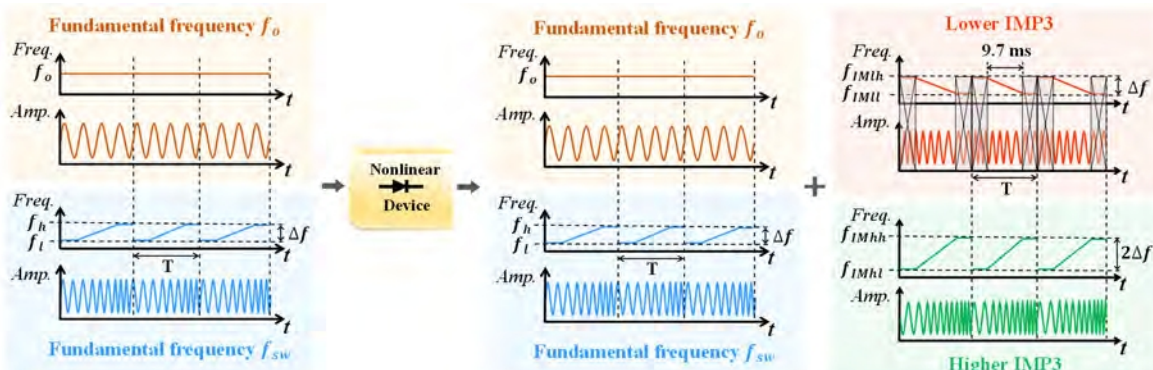


Figure 16. FMCW modulation scheme in intermodulation radar [62]. Reproduced with permission from Mishra, A., Wang, J., Rodriguez, D., and Li, C., Utilizing Passive Intermodulation Response of Frequency-Modulated Continuous-Wave Signal for Target Identification and Mapping by IEEE, 2021.

For suppressing the unwanted response, generally, diplexers and filters are used. This makes the system expensive and bulky. Thus, in [63], a frequency cancellation technique to remove unwanted responses is discussed. This technique can be used to replace the filters and diplexers in the system, making the whole architecture portable and cheap. The unwanted tones can be canceled by more than 60 dB when a perfect phase matches the undesirable and cancellation tones.

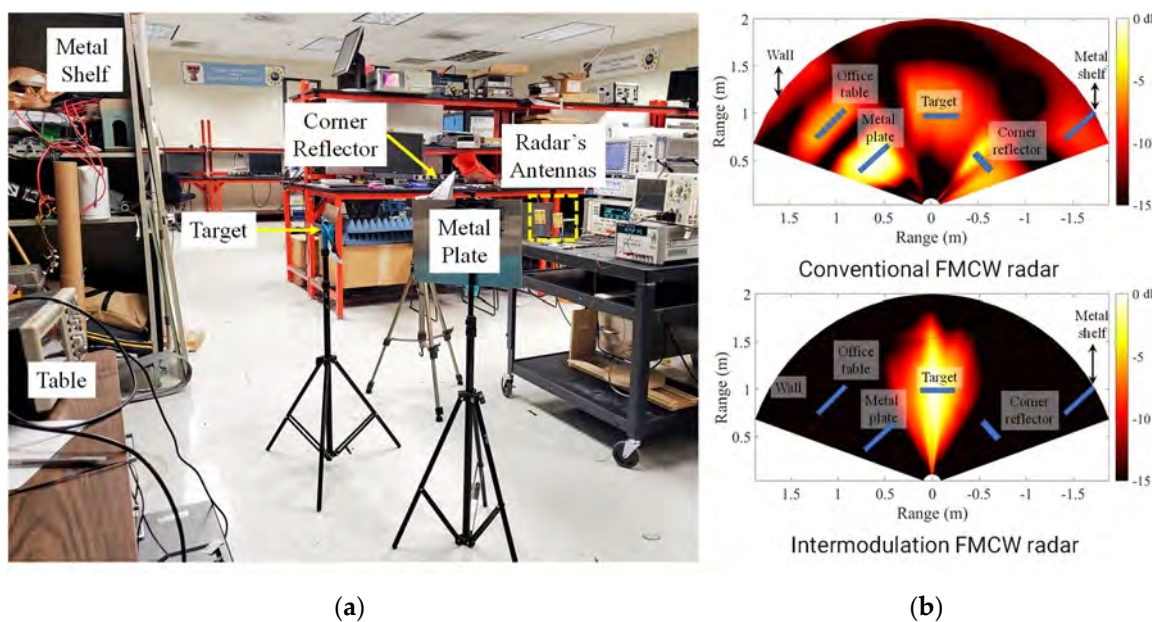


Figure 17. (a) Measurement setup; (b) mapping with intermodulation radar and comparison with a conventional FMCW radar [62]. Reproduced with permission from Mishra, A., Wang, J., Rodriguez, D., and Li, C., Utilizing Passive Intermodulation Response of Frequency-Modulated Continuous-Wave Signal for Target Identification and Mapping by IEEE, 2021.

6. Conclusions

Three types of nonlinear radars, i.e., sub-harmonic, harmonic, and intermodulation, are discussed. These radars each have advantages and disadvantages. In the case of subharmonic radar, the path loss of the desired tone is lower than the path loss of the fundamental tone at the cost of active tags and a larger receiver size. In the case of harmonic radars, higher range resolution and higher sensitivity are obtained at the price of higher path loss. Similarly, in the case of intermodulation radar, lower path loss compared with harmonic radars, more straightforward tag design, and relieved spectrum licensing requirements are possible at the expense of in-band frequency suppression and coherent signal generation. There has been extensive study of harmonic radar design. These radars have been used in the tracking of insects, animals, and birds, and locating electronics. In addition to various applications, these harmonic radars have been operated in different modes, such as Doppler, FMCW, pulsed, and many more.

Compared to the extensive work undertaken in harmonic radars, intermodulation and subharmonic radars are relatively new in the nonlinear radar field. In the past, intermodulation radars have been operated in Doppler, FSK, and FMCW modes. Due to in-band suppression of the unwanted responses, these radars need diplexers with very steep roll-offs to attenuate the unwanted responses by more than 40 to 50 dB, while allowing the response of interest to pass through with almost no attenuation. New techniques and radar architecture need to be determined that can reduce the use of diplexers, or even replace them. Currently, these intermodulation radars have been used in an indoor environment for tracking targets at a limited range. Further works can be performed in utilizing these radars in outdoor scenarios. Many different modes can be researched with this radar at various frequency levels. The active tag requirement for subharmonic radars limits their application. Therefore, works can be performed to replace active tags with passive ones. Because the path loss for a subharmonic response is lower than the path loss of harmonic or intermodulation responses, the detection range will be enhanced. Please note that the above analysis holds true when the conversion losses of the tag and fundamental frequency tone(s) have almost equal power level(s), and the antennas in radar and tag have similar gains. Because these nonlinear radars are relatively new compared to conventional radars, future works should aim to operate these radars with different modes and use them for

applications such as SAR imaging and device authentication. Currently, harmonic and subharmonic radars require expensive and bulky diplexers, which means most of their radar systems are not portable. Research needs to be conducted to replace the diplexers with a less costly and less bulky frequency cancellation circuit to improve the radar's performance. The sensitivity of these radars depends heavily on the conversion loss of the tag. Thus, improving the conversion loss and the efficiency of the tag will result in better detection at longer distances.

Author Contributions: A.M. carried out the literature review and wrote the manuscript. C.L. revised the paper and provided valuable recommendations. All authors have read and agreed to the published version of the manuscript.

Funding: The authors would like to acknowledge funding support from National Science Foundation (NSF) under grants ECCS-1808613 and ECCS-2030094.

Conflicts of Interest: The authors declare no conflict of interest.

References

1. Nallabolu, P.; Zhang, L.; Hong, H.; Li, C. Human Presence Sensing and Gesture Recognition for Smart Home Applications With Moving and Stationary Clutter Suppression Using a 60-GHz Digital Beamforming FMCW Radar. *IEEE Access* **2021**, *9*, 72857–72866. [[CrossRef](#)]
2. El Agroudy, N.; El-Shennawy, M.; Joram, N.; Ellinger, F. Design of a 24 GHz FMCW radar system based on sub-harmonic generation. *IET Radar Sonar Navig.* **2018**, *12*, 1052–1057. [[CrossRef](#)]
3. El Agroudy, N.; El-Shennawy, M.; Joram, N.; Ellinger, F. Design of a 24 GHz frequency divider-by-10 in 45 nm-silicon-on-insulator as an active reflector tag. *Electron. Lett.* **2017**, *53*, 1546–1548. [[CrossRef](#)]
4. O’Neal, M.E.; Landis, D.A.; Rothwell, E.; Kempel, L.; Reinhard, D. Tracking Insects with Harmonic Radar: A Case Study. *Am. Entomol.* **2004**, *50*, 212–218. [[CrossRef](#)]
5. Colpitts, B.; Boiteau, G. Harmonic Radar Transceiver Design: Miniature Tags for Insect Tracking. *IEEE Trans. Antennas Propag.* **2004**, *52*, 2825–2832. [[CrossRef](#)]
6. Psychoudakis, D.; Moulder, W.; Chen, C.-C.; Zhu, H.; Volakis, J.L. A Portable Low-Power Harmonic Radar System and Conformal Tag for Insect Tracking. *IEEE Antennas Wirel. Propag. Lett.* **2008**, *7*, 444–447. [[CrossRef](#)]
7. Mazzaro, G.; Martone, A.F.; McNamara, D.M. Detection of RF Electronics by Multitone Harmonic Radar. *IEEE Trans. Aerosp. Electron. Syst.* **2014**, *50*, 477–490. [[CrossRef](#)]
8. Riley, J.; Smith, A. Design considerations for an harmonic radar to investigate the flight of insects at low altitude. *Comput. Electron. Agric.* **2002**, *35*, 151–169. [[CrossRef](#)]
9. Cant, E.; Smith, A.; Reynolds, D.; Osborne, J. Tracking butterfly flight paths across the landscape with harmonic radar. *Proc. R. Soc. B Biol. Sci.* **2005**, *272*, 785–790. [[CrossRef](#)] [[PubMed](#)]
10. Tahir, N.; Brooker, G. Recent developments and recommendations for improving harmonic radar tracking systems. In Proceedings of the 5th European Conference on Antennas and Propagation, Rome, Italy, 11–15 April 2011; pp. 1531–1535.
11. Capaldi, E.A.; Smith, A.D.; Osborne, J.L.; Fahrbach, S.E.; Farris, S.; Reynolds, D.; Edwards, A.S.; Martin, A.; Robinson, G.E.; Poppy, G.M.; et al. Ontogeny of orientation flight in the honeybee revealed by harmonic radar. *Nat. Cell Biol.* **2000**, *403*, 537–540. [[CrossRef](#)] [[PubMed](#)]
12. Tsai, Z.-M.; Jau, P.-H.; Kuo, N.-C.; Kao, J.-C.; Lin, K.-Y.; Chang, F.-R.; Yang, E.-C.; Wang, H. A High-Range-Accuracy and High-Sensitivity Harmonic Radar Using Pulse Pseudorandom Code for Bee Searching. *IEEE Trans. Microw. Theory Tech.* **2012**, *61*, 666–675. [[CrossRef](#)]
13. Chioukh, L.; Boutayeb, H.; Wu, K.; Deslandes, D. Monitoring vital signs using remote harmonic radar concept. In Proceedings of the 2011 41st European Microwave Conference, Manchester, UK, 10–13 October 2011; pp. 1269–1272.
14. Chioukh, L.; Boutayeb, H.; Deslandes, D.; Wu, K. Noise and Sensitivity of Harmonic Radar Architecture for Remote Sensing and Detection of Vital Signs. *IEEE Trans. Microw. Theory Tech.* **2014**, *62*, 1847–1855. [[CrossRef](#)]
15. Singh, A.; Lubecke, V.M. Respiratory Monitoring and Clutter Rejection Using a CW Doppler Radar With Passive RF Tags. *IEEE Sens. J.* **2011**, *12*, 558–565. [[CrossRef](#)]
16. Milanesio, D.; Saccani, M.; Maggiora, R.; Laurino, D.; Porporato, M. Design of an harmonic radar for the tracking of the Asian yellow-legged hornet. *Ecol. Evol.* **2016**, *6*, 2170–2178. [[CrossRef](#)]
17. Milanesio, D.; Saccani, M.; Maggiora, R.; Laurino, D.; Porporato, M. Recent upgrades of the harmonic radar for the tracking of the Asian yellow-legged hornet. *Ecol. Evol.* **2017**, *7*, 4599–4606. [[CrossRef](#)] [[PubMed](#)]
18. Maggiora, R.; Saccani, M.; Milanesio, D.; Porporato, M. An Innovative Harmonic Radar to Track Flying Insects: The Case of Vespa velutina. *Sci. Rep.* **2019**, *9*, 11964. [[CrossRef](#)] [[PubMed](#)]
19. Mazzaro, G.J.; Martone, A.F. Multitone harmonic radar. In *SPIE Proceedings Radar Sensor Technology XVII*; SPIE: Baltimore, MD, USA, 2013; Volume 8714, p. 87140E.

20. Mazzaro, G.; Gallagher, K.A.; Owens, A.R.; Sherbondy, K.D.; Narayanan, R.M. Ultra-Wideband Harmonic Radar for Locating Radio-Frequency Electronics, Army Research Lab Adelphi Md Sensors and Electron Devices Directorate. 2014. Available online: <https://apps.dtic.mil/sti/citations/ADA614485> (accessed on 12 October 2021).

21. Gallagher, K.A.; Narayanan, R.M.; Mazzaro, G.J.; Sherbondy, K.D. Linearization of a harmonic radar transmitter by feed-forward filter reflection. In Proceedings of the 2014 IEEE Radar Conference, Cincinnati, OH, USA, 19–23 May 2014; pp. 1363–1368. [\[CrossRef\]](#)

22. Gallagher, K.A.; Mazzaro, G.J.; Nguyen, L.H.; Martone, A.F.; Sherbondy, K.D.; Narayanan, R.M. Nonlinear synthetic aperture radar imaging using a harmonic radar. In *SPIE Proceedings Radar Sensor Technology XIX*; SPIE: Baltimore, MD, USA, 2015; Volume 946, p. 946109.

23. Gallagher, K.A.; Mazzaro, G.J.; Martone, A.F.; Sherbondy, K.D.; Narayanan, R.M. Filter selection for a harmonic radar. In *SPIE Proceedings Radar Sensor Technology XIX*; SPIE: Baltimore, MD, USA, 2015; Volume 9461, p. 94610A.

24. Mazzaro, G.J.; Gallagher, K.A.; Martone, A.F.; Sherbondy, K.D.; Narayanan, R.M. Short-range harmonic radar: Chirp waveform, electronic targets. In *SPIE Proceedings Radar Sensor Technology XIX*; SPIE: Baltimore, MD, USA, 2015; Volume 9461, p. 946108.

25. Mazzaro, G.J.; Martone, A.F.; Sherbondy, K.D.; Gallagher, K.A.; Narayanan, R.M. Maximizing harmonic-radar target response: Duty cycle vs. peak power. In Proceedings of the SoutheastCon 2016, Norfolk, VA, USA, 30 March–3 April 2016; pp. 1–4. [\[CrossRef\]](#)

26. Gallagher, K.A.; Narayanan, R.M.; Mazzaro, G.J.; Martone, A.F.; Sherbondy, K.D. Static and Moving Target Imaging Using Harmonic Radar. *Electronics* **2017**, *6*, 30. [\[CrossRef\]](#)

27. Mazzaro, G.J.; Sherbondy, K.D. Hardware Simulation of Harmonic Radar Using a Transverse Electromagnetic Cell. In Proceedings of the SoutheastCon 2018, St. Petersburg, FL, USA, 19–22 April 2018; pp. 1–4. [\[CrossRef\]](#)

28. Mazzaro, G.; Sherbondy, K.D. Filter Selection for Wideband Harmonic Radar. In Proceedings of the 2019 SoutheastCon, Huntsville, AL, USA, 11–14 April 2019; pp. 1–6. [\[CrossRef\]](#)

29. Wolf, S.; McMahon, D.P.; Lim, K.S.; Pull, C.D.; Clark, S.J.; Paxton, R.J.; Osborne, J.L. So Near and Yet So Far: Harmonic Radar Reveals Reduced Homing Ability of Nosema Infected Honeybees. *PLoS ONE* **2014**, *9*, e103989. [\[CrossRef\]](#)

30. Aumann, H.M.; Emanetoglu, N.W. A wideband harmonic radar for tracking small wood frogs. In Proceedings of the 2014 IEEE Radar Conference, Cincinnati, OH, USA, 19–23 May 2014; pp. 108–111. [\[CrossRef\]](#)

31. Aumann, H.; Kus, E.; Cline, B.; Emanetoglu, N.W.; Cline, B. A low-cost harmonic radar for tracking very small tagged amphibians. In Proceedings of the 2013 IEEE International Instrumentation and Measurement Technology Conference (I2MTC), Minneapolis, MN, USA, 6–9 May 2013; pp. 234–237. [\[CrossRef\]](#)

32. Langkilde, T.; Alford, R.A. The Tail Wags the Frog: Harmonic Radar Transponders Affect Movement Behavior in Litoria lesueuri. *J. Herpetol.* **2003**, *36*, 711–715. [\[CrossRef\]](#)

33. Bottiglieri, S.; Milanesio, D.; Saccani, M.; Maggiora, R.; Viscardi, A.; Gallesi, M.M. An innovative harmonic radar prototype for miniaturized lightweight passive tags tracking. In Proceedings of the 2019 IEEE Radar Conference (RadarConf), Boston, MA, USA, 22–26 April 2019; pp. 1–6. [\[CrossRef\]](#)

34. Kiriazi, J.; Nakakura, J.; Hall, K.; Hafner, N.; Lubecke, V.; Hall, K. Low Profile Harmonic Radar Transponder for Tracking Small Endangered Species. In Proceedings of the 2007 29th Annual International Conference of the IEEE Engineering in Medicine and Biology Society, Lyon, France, 22–26 August 2007; Volume 2007, pp. 2338–2341.

35. Lavrenko, A.; Woodward, G.; Pawson, S. Parasitic Harmonic Cancellation for Reliable Tag Detection with Pulsed Harmonic Radar. In Proceedings of the 2019 IEEE Radar Conference (RadarConf), Boston, MA, USA, 22–26 April 2019; pp. 1–6. [\[CrossRef\]](#)

36. Rasilainen, K.; Viikari, V. Transponder Designs for Harmonic Radar Applications. *Int. J. Antennas Propag.* **2015**, *2015*, 565734. [\[CrossRef\]](#)

37. Aljaser, S. Miniaturization of a Low Power Harmonic Radar for UAV Use. 2019. Available online: <https://www.semanticscholar.org/paper/Miniatrization-of-a-Low-Power-Harmonic-Radar-for-Aljaser/71d91f376b163a8c86db28bd8207664d7230230a#citing-papers> (accessed on 13 October 2021).

38. Kubina, B.; Mandel, C.; Schussler, M.; Jakoby, R. Compact quasi-chipless harmonic radar sensor with a dielectric resonator antenna. In Proceedings of the 2015 IEEE MTT-S International Microwave Symposium, Phoenix, AZ, USA, 17–22 May 2015; pp. 1–3.

39. Dardari, D. Detection and accurate localization of harmonic chipless tags. *EURASIP J. Adv. Signal Process.* **2015**, *2015*, 77. [\[CrossRef\]](#)

40. Zhu, L.; Chen, P.-Y. Absolute value wireless sensing based on nonlinear harmonic analysis assisted with frequency-hopping spread spectrum. *Meas. Sci. Technol.* **2021**, *32*, 095115. [\[CrossRef\]](#)

41. Nourshamsi, N.; Hilton, C.; Vakalis, S.; Nanzer, J.A. Harmonic Micro-Doppler Detection Using Passive RF Tags and Pulsed Microwave Harmonic Radar. In Proceedings of the 2020 IEEE/MTT-S International Microwave Symposium (IMS), Los Angeles, CA, USA, 4–6 August 2020; pp. 1259–1262.

42. Ilbogi, H.; Hayvaci, H.T.; Yetik, I.S.; Yilmaz, A.E. Distinguishing electronic devices using harmonic radar. In Proceedings of the 2017 IEEE Radar Conference (RadarConf), Seattle, WA, USA, 8–12 May 2017; pp. 1527–1530. [\[CrossRef\]](#)

43. Ilbogi, H.; Hayvaci, H.T.; Yetik, I.S. Distinguishing electronic devices using fourier features derived from harmonic radar. In Proceedings of the 2017 International Conference on Electromagnetics in Advanced Applications (ICEAA), Verona, Italy, 11–15 September 2017; pp. 1502–1505.

44. Heuermann, H.; Harzheim, T.; Mühlmel, M. A Maritime Harmonic Radar Search and Rescue System Using Passive and Active Tags. In Proceedings of the 2020 17th European Radar Conference (EuRAD), Utrecht, The Netherlands, 10–15 January 2021; pp. 73–76.

45. Harzheim, T.; Mühlmel, M.; Heuermann, H. A SFCW harmonic radar system for maritime search and rescue using passive and active tags. *Int. J. Microw. Wirel. Technol.* **2021**, *13*, 691–707. [\[CrossRef\]](#)

46. Olofsson, J.; Forssen, T.; Hendeby, G.; Skog, I.; Gustafsson, F. UAS-supported Digitalized Search-And-Rescue using Harmonic Radar Reflection. In Proceedings of the 2020 IEEE Aerospace Conference, Big Sky, MT, USA, 7–14 March 2020; pp. 1–7. [\[CrossRef\]](#)

47. Meloche, F.; Albert, P.M. A lighter transponder for harmonic radar. In Proceedings of the 2006 European Radar Conference, Manchester, UK, 13–15 September 2006; pp. 233–236. [\[CrossRef\]](#)

48. Nassar, I.T.; Weller, T.M. A Compact Dual-Channel Transceiver for Long-Range Passive Embedded Monitoring. *IEEE Trans. Microw. Theory Tech.* **2014**, *63*, 287–294. [\[CrossRef\]](#)

49. Huang, H.; Sakhdari, M.; Hajizadegan, M.; Shahini, A.; Akinwande, D.; Chen, P.-Y. Toward transparent and self-activated graphene harmonic transponder sensors. *Appl. Phys. Lett.* **2016**, *108*, 173503. [\[CrossRef\]](#)

50. Lavrenko, A.; Cavers, J.K.; Woodward, G.K. Harmonic Radar with Adaptively Phase-Coherent Auxiliary Transmitters. *arXiv* **2021**, arXiv:2108.13847. Available online: <https://arxiv.org/abs/2108.13847> (accessed on 24 October 2021).

51. Mishra, A.; Li, C. A third-order harmonic radar design for mm-wave frequencies. *SPIE Radar Sens. Technol. XXV* **2021**, 11742, 117421A.

52. Droitcour, A.D.; Boric-Lubecke, O.; Lubecke, V.M.; Lin, J.; Kovacs, G.T.A. Range correlation and I/Q performance benefits in single-chip silicon Doppler radars for noncontact cardiopulmonary monitoring. *IEEE Trans. Microw. Theory Tech.* **2004**, *52*, 838–848. [\[CrossRef\]](#)

53. Ritamaki, M.; Ruhanen, A.; Kukko, V.; Miettinen, J.; Turner, L. Contactless radiation pattern measurement method for UHF RFID transponders. *Electron. Lett.* **2005**, *41*, 723–724. [\[CrossRef\]](#)

54. Saebroe, J.; Varpula, T.; Seppä, H.; Cheng, S.; Al-Nuaimi, M.; Hallbjörner, P.; Rydberg, A. Harmonic automotive radar for VRU classification. In Proceedings of the International Radar Conference “Surveillance for a Safer World”, Bordeaux, France, 12–16 October 2009; pp. 1–5.

55. Gomes, H.C.; Carvalho, N.B. The use of intermodulation distortion for the design of passive RFID. In Proceedings of the 2007 European Radar Conference, Munich, Germany, 10–12 October 2007; pp. 377–380. [\[CrossRef\]](#)

56. Mishra, A.; Li, C. 5.8-GHz ISM band intermodulation radar for high-sensitivity motion-sensing applications. In Proceedings of the 2018 IEEE Radio and Wireless Symposium (RWS), Anaheim, CA, USA, 15–18 January 2018; pp. 4–6. [\[CrossRef\]](#)

57. Mishra, A.; Song, C.; Xu, W.; Li, C. Investigation of unique broadband nonlinear RF response of electronic devices. In Proceedings of the 2018 IEEE Radio and Wireless Symposium (RWS), Anaheim, CA, USA, 15–18 January 2018; pp. 281–283. [\[CrossRef\]](#)

58. Mishra, A.; Li, C. A Low Power 5.8-GHz ISM-Band Intermodulation Radar System for Target Motion Discrimination. *IEEE Sens. J.* **2019**, *19*, 9206–9214. [\[CrossRef\]](#)

59. Li, C.; Wang, J.; Rodriguez, D.; Mishra, A.; Peng, Z.; Li, Y. Portable Doppler/FSK/FMCW Radar Systems for Life Activity Sensing and Human Localization. In Proceedings of the 2019 14th International Conference on Advanced Technologies, Systems and Services in Telecommunications (TELSIKS), Nis, Serbia, 23–25 October 2019; pp. 83–93.

60. McDonnell, W.; Mishra, A.; Li, C. Comprehensive Vital Sign Detection using a Wrist Wearable Nonlinear Target and a 5.8-GHz ISM Band Intermodulation Radar. In Proceedings of the 2020 IEEE Radio and Wireless Symposium (RWS), San Antonio, TX, USA, 26–29 January 2020; pp. 123–126. [\[CrossRef\]](#)

61. Mishra, A.; McDonnell, W.; Wang, J.; Rodriguez, D.; Li, C. Intermodulation-Based Nonlinear Smart Health Sensing of Human Vital Signs and Location. *IEEE Access* **2019**, *7*, 158284–158295. [\[CrossRef\]](#)

62. Mishra, A.; Wang, J.; Rodriguez, D.; Li, C. Utilizing Passive Intermodulation Response of Frequency-Modulated Continuous-Wave Signal for Target Identification and Mapping. *IEEE Sens. J.* **2021**, *21*, 17817–17826. [\[CrossRef\]](#)

63. Tang, D.; Mishra, A.; Li, C. Intermodulation Radar with Dynamic Fundamental Tone Cancellation for Linearity Improvement. In Proceedings of the 2021 IEEE Topical Conference on Wireless Sensors and Sensor Networks (WiSNeT), San Diego, CA, USA, 17–20 January 2021; pp. 63–65.